RSC Advances

PAPER

View Article Online
View Journal | View Issue

Open Access Article. Published on 20 February 2014. Downloaded on 4/21/2025 6:47:34 PM.
This article is licensed under a Creative Commons Attribution 3.0 Unported Licence.

Cite this: *RSC Adv.*, 2014, **4**, 12729

Morphological changes of gold nanoparticles due to adsorption onto silicon substrate and oxygen plasma treatment†

Katarzyna Winkler,[a] Tomasz Wojciechowski,[b] Malwina Liszewska,[ac] Ewa Górecka[d] and Marcin Fiałkowski*[a]

Received 17th January 2014
Accepted 18th February 2014

DOI: 10.1039/c4ra00507d

www.rsc.org/advances

Deposition of gold nanoparticles (AuNPs) on a solid substrate followed by oxygen plasma treatment is a commonly used protocol for surface functionalization. Surprisingly, the effect of the deposition process and oxygen plasma on the morphology of the AuNPs is usually overlooked in research. Here, we investigated morphological changes caused by (i) adsorption of small ligand-capped AuNPs (~5 nm in diameter) onto a silicon substrate and (ii) subsequent oxygen plasma treatment. AuNPs coated with positively and negatively charged as well as uncharged ligands have been investigated. It is found that upon the adsorption the AuNPs undergo plastic deformations and their shapes can be approximated by spherical caps. The degree of the deformation depends strongly on the AuNP coating. During the plasma treatment the AuNPs behave like droplets of a non-wetting liquid, exhibiting the ability to move and merge. We argue that the AuNP coarsening is dominated by the diffusion coalescence mechanism and show that time evolution of the surface AuNP density follows the Smoluchowski coagulation equation. The diffusivity of the AuNP scales with its mass as $D(m) \sim m^{-\alpha}$ with $\alpha = 2.6$.

Introduction

Nanoparticles of noble metals, especially gold ones (AuNPs), have been investigated as promising materials in the fields of chemistry, physics, materials science, biology, and medical applications. Of particular interest are two-dimensional (2D) structures formed by AuNPs deposited on solid substrates. Such structures are widely employed in light emitting devices, solar cells, antireflective films, as catalysts for carbon nanotubes growth, or for the vapor–liquid–solid growth of inorganic nanowires.[1] AuNPs are covered with organic protecting layer that prevents their aggregation in solution. After the deposition this organic layer is usually no longer needed and often has to be removed from the AuNPs. The removal of the organic material involves either thermal or plasma treatment. In the present studies we focus on the latter cleaning method.

The treatment with oxygen plasma is a technique utilized both in a purification of bulk gold[2] and AuNPs.[3–5] In the highly reactive gas, organic compounds are oxidized and removed as a carbon, sulfur and nitrogen oxides by a vacuum system. Surprisingly, despite of popularity and usefulness of the plasma treatment, the knowledge about processes which take place in a plasma cleaner is poor. There are conflicting opinions in the literature on this issue. In particular, the discrepancies concern the impact of the oxygen plasma on the structure of the AuNP deposit. Some authors report that long exposure of AuNPs to oxygen flow did not alter neither their regular structure nor initial arrangement of the AuNPs on the substrate.[4,6] According to other reports, even short-time and low-power (10 W) plasma cleaning alters significantly the initial morphology of the deposit, causing coarsening of the AuNPs.[7] One can also find opinion that high oxygen plasma power (>300 W) is needed to destroy the structure of the deposit. In this case, breaking of a linkage between the AuNPs and a SiO_x substrate takes place, resulting in the removal of AuNPs from the surface.[3] Given such diverse opinions on the effects of the oxygen plasma treatment, it is obvious that the nature of this process is far from being well-understood.

This is the purpose of our work to investigate the effects of both the deposition and plasma cleaning process, and elucidate their impact on the morphology of the AuNPs. We apply low-power oxygen plasma to the AuNPs deposited on silicon substrate using a recently developed technique.[8] This technique employs direct adsorption of charged AuNPs on a substrate, and facilitates obtaining coatings of desired density.

[a]*Institute of Physical Chemistry of the Polish Academy of Sciences, Kasprzaka 44/52, 01-224 Warsaw, Poland. E-mail: mfialkowski@ichf.edu.pl; Fax: +48-22-343-3333; Tel: +48-22-343-2067*

[b]*Institute of Physics of the Polish Academy of Sciences, Lotników 32/46, 02-668 Warsaw, Poland*

[c]*Institute of Optoelectronics, Military University of Technology, Kaliskiego 2, 00-908 Warsaw, Poland*

[d]*Department of Chemistry, University of Warsaw, Żwirki i Wigury 101, 02-089 Warsaw, Poland*

† Electronic supplementary information (ESI) available: XRD spectra and SEM images. See DOI: 10.1039/c4ra00507d

Open Access Article. Published on 20 February 2014. Downloaded on 4/21/2025 6:47:34 PM.
This article is licensed under a Creative Commons Attribution 3.0 Unported Licence.

Experimental section

Materials

Sulfuric acid and hydrogen peroxide were purchased from Chempur. *N*,*N*,*N*-Trimethyl(11-mercaptoundecyl)ammonium chloride ($HS(CH_2)_{11}N(CH_3)_3^+Cl^-$, TMA), was synthesized according to the known procedure.[9] We employed as solvents acetone and methanol from Chempur, and deionized water (15 MΩ). All other reactants were purchased from Sigma-Aldrich. The reagents were all analytical grade and used without further purification. The silicon wafers (orientation 100) were purchased from Cemat Silicon. Before use, the wafers were cut manually into stripes and cleaned by sonication in water and then in acetone. Next, the plates were immersed in a freshly prepared piranha solution (3 volumes of 98% H_2SO_4 and 1 volume of 30% H_2O_2) for 3 h. Finally, the plates were rinsed with deionized water and then with methanol, and dried in air. Note that the outer layer of the silicon plate is readily oxidized to SiO_2. However, it is not known neither what portion of the surface is oxidized nor the depth of the oxidized layer. For this reason, in the present work we refer to the substrate as to the silicon or SiO_x one.

Preparation of AuNPs

In our experiments we examined both hydrophobic and hydrophilic (positively or negatively charged) gold nanoparticles. The uncharged AuNPs were synthesized according to the procedure of Jana and Peng,[10] in which hydrophobic AuNPs covered with dodecylamine (Au@DDA NPs) are formed. The obtained Au@DDA NPs had average radius of 2.5 nm with polydispersity 0.71 nm, as determined from the SAXS spectrum of the AuNP solution.

To provide a positive charge on the NPs, the hydrophobic amine ligands were replaced with the ω-functionalized alkanethiol, TMA. To carry out the ligand exchange reaction, we applied the following procedure: from the toluene solution (10 g, 7.05 mM, 0.075 mmol Au) the Au@DDA NPs were precipitated with methanol (70 mL), then dissolved in chloroform (15 mL) and added dropwise to the solution of TMA (30 mg, 0.11 mmol) in methanol (5 mL). The mixture was stirred overnight. After this time and after addition of isopropanol (2 mL) the AuNPs were precipitated with hexane and centrifuged (30 min, 7000 rpm). Supernatant was decanted and the black precipitate of AuNPs was dissolved in methanol (1.5 mL) and isopropanol (1.5 mL), precipitated with hexane (~40 mL), and centrifuged (15 min, 6000 rpm). The dissolution and precipitation process was repeated five times. Eventually, the purified and dried AuNPs were dissolved in 35 mL of deionized water yielding a 0.73 mg mL^{-1} gold solution. The average radius of the metal core of the Au@TMA NPs, determined from the SAXS spectrum of the AuNP solution, was 2.5 nm with the polydispersity 0.43 nm. The thickness of the TMA protecting monolayer on the AuNPs, calculated using ChemSketch, was about 1.8 nm.

The negatively charged AuNPs were prepared in an analogous manner to the positively charged ones. We used the same procedure but applied mercaptoundecanoic acid (MUA) instead of TMA. In the final step we dissolved the Au@MUA NPs in methanol.

Deposition of AuNPs onto silicon substrate

The TMA-covered AuNPs were deposited onto silicon plate with the ionic-strength controlled method,[8] which facilitated obtaining coatings of different densities. In our experiments we investigated two types of the AuNP coatings: low- and high-density ones. To deposit the AuNPs, a silicon plate was immersed for 10 min in 4 mL of aqueous solution of AuNPs (0.18 mg mL^{-1}) and sodium chloride (1 mM and 2 M for the low- and high-density coating, respectively). The slide was then removed from the solution and rinsed with deionized water to wash out the salt and residual AuNPs that were not adsorbed on the surface. Finally, the slide was dipped in methanol for about 10 s, and dried by placing it in a vertical position on a filter paper.

In experiments where drop casting instead of ionic-strength controlled method was used, we simply put a drop of AuNP solution on the silicon, waited until all solvent evaporate, and then rinsed silicon plates consecutively with water and methanol and dried in the air.

Study of the evolution of the surface droplet density

The droplet (AuNP) surface densities were determined independently for each plasma treatment time. Silicon stripes covered with the AuNP coating were kept in the plasma cleaner for prescribed time and then analyzed with SEM. The droplet surface densities were calculated as averages for three independent experiments and for three SEM images in every experiment.

Instrumentation

Surfaces covered with the AuNPs were analyzed using field emission scanning electron microscopy (FE-SEM) with Neon 40-Auriga Carl Zeiss apparatus, applying 5 kV beam voltage. The plates covered with the AuNPs were treated with oxygen plasma for various times at 29.6 W in Harrick Plasma Cleaner PDC-002 (Harrick Plasma, USA). Small angle X-ray scattering (SAXS) were carried out using Bruker Nanostar system; the patterns were registered with Vantec 2000 area detector. The CuK ($\alpha = 1.54$ Å) radiation was used. Samples were placed in Lindemann capillaries (1.5 mm in diameter). The signal intensities were obtained through integration of the 2D patterns over an azimuthal angle. XRD spectra were recorded using Bruker D8 Discover equipped with Vantec linear detector and at CuKα radiation in reflection geometry. All measurements were carried out at room temperature. The percentage surface coverage, φ, was determined using histogram tool in a graphic software. The AuNP number and projected radii were determined manually.

Results and discussion

Morphology of the AuNP deposit

The morphology of the TMA-covered AuNPs deposited on the silicon substrate was investigated with SEM microscopy. In the case of the low-density coating the AuNPs were distributed

 This journal is © The Royal Society of Chemistry 2014

Open Access Article. Published on 20 February 2014. Downloaded on 4/21/2025 6:47:34 PM.
This article is licensed under a Creative Commons Attribution 3.0 Unported Licence.

uniformly (Fig. 1a) and formed a sparse layer. The percentage surface coverage, that was calculated as the ratio of the sum of the projected areas of all objects to the area of the image analyzed, was $\varphi \sim 7\%$. In the case of the high-density coatings the AuNPs were arranged in a network of connected patches (Fig. 1b), covering about 20% of the surface.

In both the cases, the average projected (apparent) radius of the adsorbed AuNPs, R_a, calculated from the SEM images, was $R_a = (3.94 \pm 0.08)$ nm. This value of the projected radius was significantly larger than that of the non-adsorbed AuNPs in the solution, $R_0 = 2.5$ nm, calculated based on SAXS measurements. Analysis of the side-view SEM images revealed that the increase of the projected radius was caused by the deformation of the shapes of the AuNPs. As can be seen in Fig. 2a, *the AuNPs attached to the surface are clearly flattened and resemble portions of spheres*. It was also found that the average contact angle, θ_a, of the AuNPs was $\theta_a = (54.3 \pm 3.9)^\circ$.

The flattening of the metal cores that occurs during the adsorption process should be taken into account when estimating sizes of AuNPs based on SEM or TEM images. The shapes of the adsorbed particles can also significantly affect physical and chemical properties of the metal coating, such as its catalytic surface area. Thus, it is quite surprising that the effect of the deposition on the AuNP core is largely overlooked. In the following, we demonstrate that the shapes of the adsorbed AuNPs can be approximated as spherical caps. To show this, we start with the observation that the average volume of the AuNPs adsorbed on the substrate is equal to that of the average volume, V_{av} (see Fig. 3a), of the AuNPs in the bulk solution,

$$V_{av} = \frac{4}{3}\pi R_0^3. \quad (1)$$

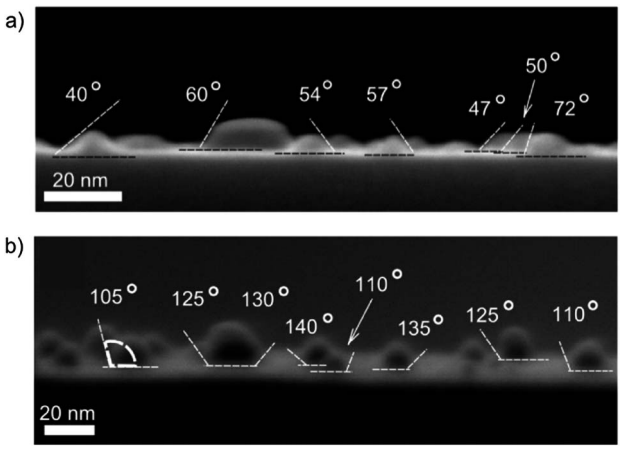

Fig. 2 Side-view SEM image of the AuNPs deposited on the plate (a) before and (b) after the plasma cleaning. Values of the contact angles for selected AuNPs are shown.

The average volume of the AuNPs adsorbed on silicon is calculated as a volume of the spherical cap, V_{cap}, that is the following function of the contact angle, θ_a, and the radius, R, of the sphere (see Fig. 3b):

$$V_{cap} = \frac{\pi}{3}R^3(2 - 3\cos\theta_a + \cos^3\theta_a). \quad (2)$$

The condition $V_{av} = V_{cap}$ yields the following expression for the radius R:

$$R = R_0 4^{1/3}(2 - 3\cos\theta_a + \cos^3\theta_a)^{-1/3}. \quad (3)$$

The projected area of the AuNP is the base of the cap, and its radius, R_a, is related to the radius R and the contact angle θ_a through the following relation:

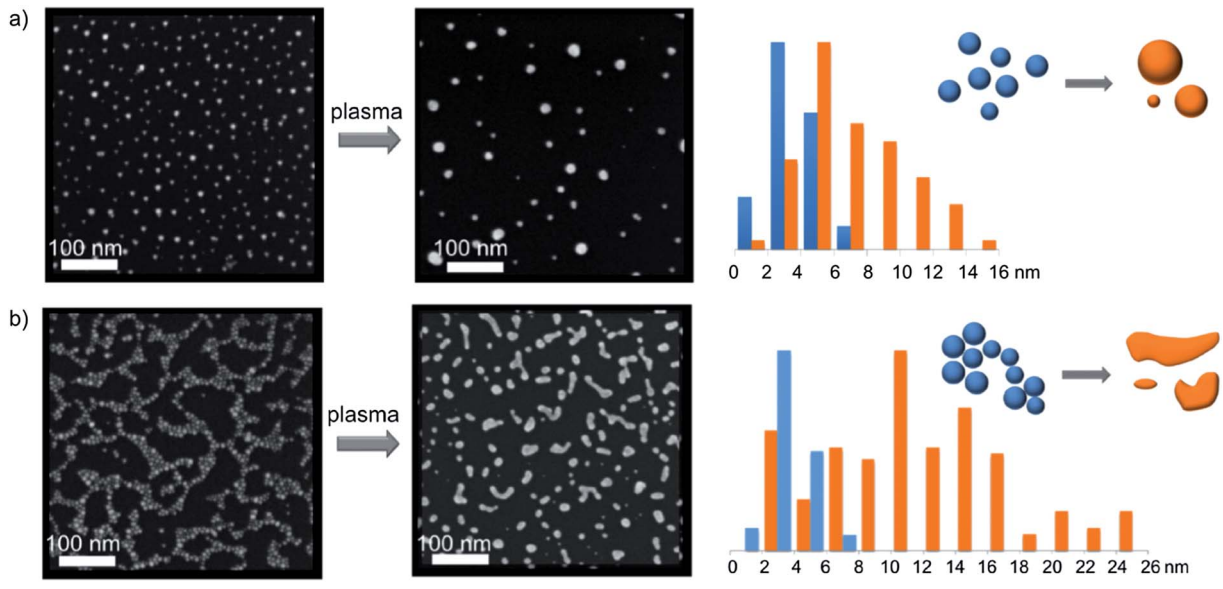

Fig. 1 SEM images illustrating the effect of the plasma treatment on the AuNPs deposited on a silicon plate for the low-density (a), and high-density (b) coatings. The histograms show distributions of the AuNP projected radii before (blue) and after (orange) the plasma treatment. For the high-density coating the radii were calculated as radii of spheres of the same projected area.

Open Access Article. Published on 20 February 2014. Downloaded on 4/21/2025 6:47:34 PM.
This article is licensed under a Creative Commons Attribution 3.0 Unported Licence.

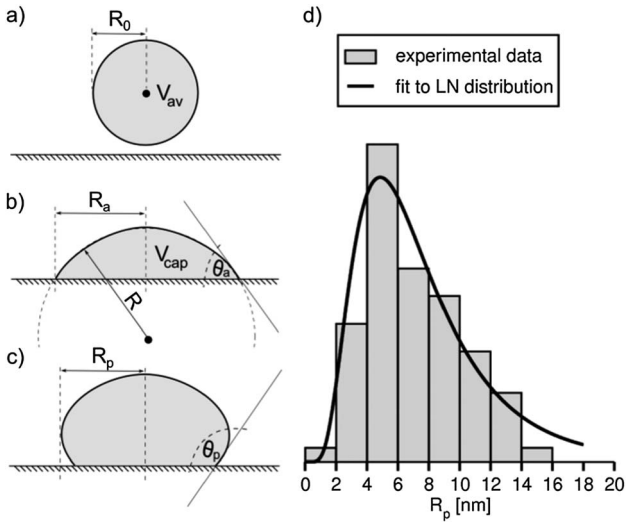

Fig. 3 Geometry of the AuNP (a) in the solution, (b) after deposition on the substrate, and (c) after the plasma treatment. (d) Distribution of the projected radii, R_p, of the AuNPs after the plasma treatment. The solid line is the fit of the log-normal (LN) distribution.

$$R_a = \begin{cases} R\sin\theta_a, & \text{for } \theta_a \le 90^\circ \\ R, & \text{for } \theta_a > 90^\circ \end{cases} \quad (4)$$

The projected radius, R_a, is a quantity that is obtained directly from the SEM images. Eqn (4) enables determination of the contact angle, θ_a, as a function of the ratio R_a/R_0. For $R_0 = 2.5$ nm and $R_a = (3.94 \pm 0.08)$ nm eqn (4) yields $\theta_a = (62.5 \pm 4.4)^\circ$. It follows that – within statistical errors – this value agrees with that determined directly based on the side-view SEM images. This result supports the assumption that the shapes of the deposited AuNPs can be approximated by spherical caps. Thereby, it rules out the possibility that these shapes visible in the SEM images may be due to the organic material present in the bottom of the particles.

The most plausible cause of the observed shape deformation of the AuNPs is the electrostatic attraction between the positively charged TMA ligands and negatively charged surface of the SiO_x substrate. The extent of the deformation indicates that – surprisingly – the AuNP core becomes plastic under the stresses caused by the electrostatic forces. To examine the effect of the electrostatic interaction on the resulting NP shape we carried out experiments with NPs coated with both positively (TMA) and negatively charged (MUA) and uncharged (DDA) ligands. All types of the AuNPs were deposited with the same, drop casting technique (the ionic-strength controlled method can be applied only for positively charged coating). To quantify the deformation degree we calculated the ratio R_a/R_0 of the projected radius after the deposition to the radius in a bulk solution, and the contact angle, θ_a. The contact angle was calculated from eqn (4) based on the R_a/R_0 ratio. The results are collected in the Table 1. We found that the positively charged AuNPs undergo the most significant deformations. Their average projected radius is more than 150% of that in bulk solution. For the DDA-coated uncharged NPs the degree of deformation is smaller (134%). It can be explained by lower attraction between the AuNP ligand and the substrate surface. The negatively charged Au@MUA NPs that are electrostatically repelled from the silicon surface, are only slightly deformed, and their projected radii increase caused by the deposition is less than 10%. We observed that the contact angle increased with decreasing attraction between the NP and the substrate. The value of θ_a changed from 62.2° (corresponding to the "wetting" geometry) for positively charged TMA ligands to 113° ("non-wetting" geometry) for negatively charged MUA ligands. The results shown in the Table 1 prove that the electrostatic interaction between organic ligands and solid substrate has a profound effect on the shape of the deposited AuNPs. Electrostatic forces are strong enough to make gold atoms move within the nanoparticle, and lead to its significant deformation.

The analysis of the effect of plasma on the AuNPs shape presented in following sections was done for Au@TMA NPs deposited using the ionic-strength controlled method that allowed obtaining coatings of various densities. We checked whether the morphology of the AuNPs deposit obtained with this method is the same as for the simple drop casting technique. It was found (see Table 1) that the average projected radius for the drop casting method was (3.95 ± 0.06) nm. This value agrees very well with that obtained for the ionic-strength controlled method, (3.94 ± 0.08) nm. Thus, the changes of the AuNPs shape do not depend on the deposition technique used.

The structure of the most deformed NPs (Au@TMA) deposited on silicon substrate was also investigated by X-ray diffraction (XRD) analysis. The XRD studies revealed that – despite of significant deformation of the initial spherical shapes – the adsorption process did not destroy the crystal structure (fcc) of the AuNPs. The XRD pattern of the AuNP coating displayed one broad peak at $2\theta = 38.3^\circ$, corresponding to the Au(111) plane (see Fig. S1 in the ESI†).

Table 1 Characterization of the deformation degree for ligand-coated AuNPs deposited on SiO_x substrate

AuNP type	R_0, radius in bulk (nm)	R_a, projected radius (nm)	R_a/R_0	Contact angle (deg.)
Au@TMA[a]	2.50	3.94 ± 0.08	1.58	62.5 ± 4.4
Au@TMA[b]	2.50	3.95 ± 0.06	1.58	62.2 ± 3.3
Au@DDA[b]	2.53	3.40 ± 0.07	1.34	82.4 ± 3.3
Au@MUA[b]	2.16	2.35 ± 0.04	1.09	112.9 ± 7.4

[a] Deposited using the ionic-strength controlled method. [b] Deposited using drop casting method.

 This journal is © The Royal Society of Chemistry 2014

Open Access Article. Published on 20 February 2014. Downloaded on 4/21/2025 6:47:34 PM.
This article is licensed under a Creative Commons Attribution 3.0 Unported Licence.

Morphology of the AuNP deposit after the plasma treatment

After the plasma treatment, a significant coarsening of the AuNPs was observed both for the low- and high-density coating. In the case of the low-density coating the resulting particles possessed circular projected shapes of the average radius $R_p = (7.51 \pm 0.36)$ nm (see Fig. 1a). The sizes of the particles span from about 4 to 30 nm. The percentage surface coverage, φ, decreased about 2.3 times (from ~7 to ~3%). After the plasma treatment, the number density of the AuNPs was reduced 5.2 times. In the case of high-density coatings, the plasma cleaning led to the formation of objects possessing rather irregular and elongated shapes, up to 70 nm in length. The average projected particle radius was about 12 nm. (Due to irregular shapes of plasma-treated AuNPs, their radii were calculated as radii of spheres of the same projected area.) Interestingly, the plasma treatment resulted in 2.2-fold decrease of the initial surface coverage (from ~20 to ~9%) that is close to that observed for the low-density coatings. The number density of the AuNPs on the substrate was 6.1 times smaller than before the process of the plasma treatment.

From the side-view SEM images (see Fig. 2b and 3c) it was found that the average contact angle, θ_p, of the particles formed after the plasma treatment was $\theta_p = (122.5 \pm 4.5)^\circ$. However, only small- and medium-sized particles (<20 nm) had shapes that could be approximated by portions of spheres. Larger particles exhibited less regular shapes. Despite of visible change in the shape of the AuNPs, their crystallographic structure is preserved. The XRD pattern after the plasma treatment displayed a broad peak at $2\theta = 38.3^\circ$ that corresponds to the Au(111) plane (see Fig. S1†).

The resulting distribution of the projected radii of the droplets was investigated. In our studies, we analyzed the low-density coatings because only in this case the projections of the AuNPs possessed well-defined circular shapes (see Fig. 1a). Distribution of the droplet radii after the plasma treatment process exhibited a clear positive skewness, as shown in Fig. 3d. To quantify this distribution, we fitted to the obtained frequency the log-normal (LN) distribution function given by

$$f_{LN}(R_p) = \frac{1}{\sqrt{2\pi}\sigma R_p}\exp\left[-\frac{1}{2}\left(\frac{\ln R_p - \ln \mu}{\ln \sigma}\right)^2\right], \quad (5)$$

where $\ln \mu$ and $\ln \sigma$ are the mean and standard deviation of $\ln R_p$, respectively. The fitting procedure yielded $\mu = 6.590$ nm and $\sigma = 1.824$. To check whether the frequencies shown in Fig. 3d follow the LN distribution, the chi-square goodness-of-fit test was carried out. For the LN distribution function, given by eqn (5) fitted to the experimental data, the test statistic was $\chi^2 = 4.492$. For four degrees of freedom $P(\chi^2 > 4.492) = 0.34$. It follows that the P-value > 0.05, and that the hypothesis that the LN distribution describes the observed frequencies is accepted. Note also that the average size of the AuNPs, determined from the formula $\mu \exp[\ln^2(\sigma)/2]$, is 7.89 nm and agrees fairly well with R_p obtained directly from the SEM images (7.51 nm).

Evolution of the AuNP coating during the plasma treatment

The growth of the AuNPs during the plasma cleaning can occur through two different mechanisms: *first*, the growth can be caused by migration of single Au atoms between the particles. This process is often referred to as the Ostwald ripening (OR).[11,12] During OR the diffusion-mediated mass transport of atoms allows for the growth of large particles at the expense of small ones. OR mechanism governs thermal sintering processes of metal clusters,[13–15] and coarsening of Ag/Ag(111) and Cu/Cu(111) adatom islands.[16] *Second*, the growth of the AuNPs can occur when the particles are free to move on the substrate surface and undergo collisions that lead to the coalescence. This second process is expected to be operative for small clusters that exhibit ability to move on a substrate.[15,17,18] This process is also referred to as the Smoluchowski Ripening (SR) because of the long-established Smoluchowski coagulation rate equation.[19] The SR mechanism governs, for instance, growth of Ag/Ag(100) and Cu/Cu(100) islands.[20,21] Both SR and OR processes have recently been reported[15] to be involved in the sintering of metal clusters. In the following, we discuss theoretical predictions of both OR and SR models and compare them with experimental data.

Smoluchowski ripening

Let us denote the surface density of the droplets of mass m as $n_m(t)$. Assuming that the coarsening occurs only through collisions between pairs of the NPs, the evolution of $n_m(t)$ is governed by the following Smoluchowski coagulation rate equation:[19]

$$\frac{d}{dt}n_m(t) = \frac{1}{2}\sum_{m'} k(m, m-m')n_{m'}(t)n_{m-m'}(t) - n_m(t)\sum_{m'} k(m, m')n_{m'}(t) \quad (6)$$

where $k(m, m')$ denotes the rate constant of collisions between two droplets of masses m and m'. Assuming that the diffusing droplets are spatially uncorrelated, in 2D the rate constant is given by the relation[22]

$$k(m, m') = D(m) + D(m'), \quad (7)$$

where $D(m)$ is diffusion coefficient of the droplet of mass m. In the Smoluchowski's model of coagulation, it is assumed that the diffusion coefficient is related to the mass of the droplet by

$$D(m) = D^* m^{-\alpha}, \quad (8)$$

where D^* is a temperature-dependent prefactor, and α is an exponent that depends on specific mechanism governing the movement of the droplets. So far, the scaling relationship given by eqn (8) has been investigated only for the diffusion of flat (2D) clusters composed of atoms adsorbed on a solid surface. Theoretical studies based on the mean-field approach predicted[23] values of the exponent $\alpha = 1/2$, 1, and 3/2 for, respectively, the "evaporation condensation", "terrace coarsening", and the "perimeter diffusion" mechanisms of the cluster

Open Access Article. Published on 20 February 2014. Downloaded on 4/21/2025 6:47:34 PM.
This article is licensed under a Creative Commons Attribution 3.0 Unported Licence.

movement. Experimentally determined values of the exponent alpha have been reported in the range $0 < \alpha < 2$.[20,21,24,25] *To date, there is however no theoretical model predicting the scaling relationship for nano-sized droplets performing diffusive motion on a solid substrate*. We will show that predictions of the SR model fit well the experimental data, and provide – for the first time – estimation of the exponent α.

The Smoluchowski rate equation can be transformed to an equation for the evolution of the average droplet density, $n_{av}(t)$,

$$\frac{d}{dt}n_{av}(t) = -{n_{av}}^2(t)D_{av}, \quad (9)$$

where $n_{av} = \Sigma_m n_m$, and $D_{av} = \Sigma_m D(m)n_m/n_{av}$ are, respectively, the average density and the average diffusion coefficient of the droplets. Making use of the fact that mass is proportional to the volume of the droplet, and that the total mass of the AuNP deposit is conserved, *viz.*

$${n_{av}}^0{V_{av}}^0 = n_{av}V_{av}, \quad (10)$$

where ${n_{av}}^0$ is the average droplet density before the plasma treatment, under the assumption that $D_{av} \approx D(n_{av})$, the scaling relation (8) is transformed into the form

$$D_{av} = D^*\left(\frac{V_{av}}{{V_{av}}^0}\right)^{-\alpha} = D^*\left(\frac{{n_{av}}^0}{n_{av}}\right)^{-\alpha}. \quad (11)$$

By combining eqn (10) and (11) one gets

$$\frac{d}{dt}n_{av} = -{n_{av}}^2\left(\frac{n_{av}}{{n_{av}}^0}\right)^{\alpha}D^*. \quad (12)$$

Integration of eqn (12) yields the following equation for the evolution of the surface droplet density:

$$n_{av}(t) = {n_{av}}^0\left[1 + (1+\alpha)D^*{n_{av}}^0 t\right]^{-\beta} \text{ with } \beta = \frac{1}{1+\alpha}. \quad (13)$$

To check whether the morphology of the AuNP deposit changes in accord with predictions of eqn (13), we determined experimentally the surface droplet density for five exposition times, $t = 0$, 15, 30, 120, and 360 s. The data are shown in Fig. 4. Fitting of eqn (13) to the experimental data provided the exponent $\alpha = 2.59 \pm 0.12$. This value is slightly larger than values of α reported[20,21,24,25] for flat clusters ($0 < \alpha < 2$) comprising 10^1–10^2 adatoms. This result is not surprising because the mechanism underlying movement of the nano-sized droplets composed of $\sim 10^4$–10^5 atoms is expected to be different. The fitting procedure allowed also estimation of the prefactor $D^* \sim 2 \times 10^{-12}$ cm^2 s^{-1}. This value corresponds to the diffusivity of the AuNPs of the diameter $\sim$5 nm.

To discuss the AuNP diffusion mechanism, let us note that the temperature of the silicon plate during the plasma treatment was close to room temperature. (The plate's temperature was determined immediately after its removal from the plasma cleaner chamber.) The obtained value of the diffusion coefficient is of the same order of magnitude as that of Pt/Al_2O_3 clusters of the size $\sim$3.5 nm in 600 °C,[18] and that of Au atoms on

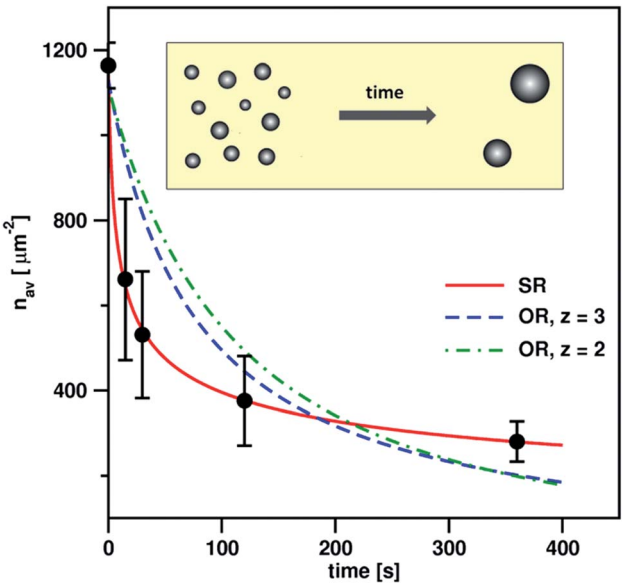

Fig. 4 Number of the AuNPs after plasma treatment as a function of the time of the process.

mica in temperature range 300–500 °C.[14] It is also several orders of magnitude larger than those measured[21,24] for small adatom clusters at room temperature (10^{-18}–10^{-15} cm^2 s^{-1}). From the above comparison it follows that the obtained diffusion coefficient of AuNPs is too large to result from a thermal Brownian motion. Thus, it is likely that the diffusion of the AuNPs during the plasma treatment is not an thermal-induced process occurring in thermodynamic equilibrium, but other mechanism is operative. During the plasma treatment, the AuNPs are bombarded with both high-energy ions and uncharged molecules. These objects immediately remove the organic coating from the AuNPs core. Then, upon collisions, transfer part of their kinetic energy to the surface atoms of the AuNPs. This can lead to the liquefaction of the gold nanoparticle (or of its surface layer in the case of a large nanoparticle). Most probably, also diffusion of the AuNPs on the surface is enhanced by collisions with high energy particles of plasma through the mechanism similar to that in ion- and electron-irradiation[26] induced growth of metal nanoclusters.

Ostwald ripening

When OR is the dominant growth mechanism the average radius of the droplet, $\langle R \rangle$, follows the relation[12]

$$\langle R \rangle^z - \langle R_0 \rangle^z = ct, \quad (14)$$

where $\langle R_0 \rangle$ denotes the average initial radius, c is a constant, and z is the exponent. The value of z depends on the specific mechanism of the mass transport. For three-dimensional growth clusters on a solid substrate one expects[12,14] $2 < z < 3$. Making use of the total mass conservation condition given by relation (10), and assuming that the droplet volume is proportional to the third power of its radius, one gets

 This journal is © The Royal Society of Chemistry 2014

Open Access Article. Published on 20 February 2014. Downloaded on 4/21/2025 6:47:34 PM.
This article is licensed under a Creative Commons Attribution 3.0 Unported Licence.

$$n_{av}(t) = n_{av}{}^{0}[1 + cR_0{}^{-z}t]^{-3/z}. \quad (15)$$

Interestingly, note that the SR and OR model predict essentially similar functional dependence of the surface droplet density on time. Formulas (13) and (15) become identical for $\alpha = z/3 - 1$. Fits of eqn (15) to the experimental data obtained for $z = 2$ and $z = 3$ are shown in Fig. 4.

Discussion

Results presented in Fig. 4 lead to conclusion that the coarsening of the AuNPs is dominated by the diffusion-coalescence mechanism. Formula for $n_{av}(t)$ derived from the SR model fits the experimental data significantly better than that predicted by OR. What is important, the fit of eqn (13) gives reasonable value of the diffusivity of the droplets that is similar to those reported in literature.[18] Also, the obtained value of the exponent α indicates that the diffusion coefficient is decreasing rapidly with the size of the particle, which is in line with experimental observations.[18] These facts show that the SR model provides a reliable description of the coarsening process.

The second argument in favour of the SR mechanism follows from the analysis of the droplet morphology. Namely, the observed significant increase of the contact angle, from 54 to 123°, suggests that during the plasma treatment outer portions of the AuNPs are melting, and their final shapes result to a great extent from minimization of the surface energy. Such transition into liquid state can enable the AuNPs to move on the surface and coalesce upon collisions. As can be seen in the SEM image of the high-density coating (Fig. 1b), after the plasma treatment the majority of the droplets possess complex, irregular shapes. Most probably, such morphology results from partial fusion of the neighbouring AuNPs, accompanied by breakage of the initial network-like structure. Note that similar structures composed of partially fused droplets, displaying sharp cusps, were observed also in the low-density coating (see Fig. ESI-2†). It is rather unlikely that the OR process, which eliminates highly curved surfaces, could produce the structures observed after the plasma treatment.

It has recently been argued[13,15] that the mechanism governing the cluster growth cannot be determined solely from the particle size distribution. Nevertheless, its form can be a source of information about possible processes involved in the coarsening. When OR is the dominant growth mechanism then asymmetric size distributions with negative skewness are observed.[11,12,27] On the other hand, the coalescence-induced growth results in an asymmetric size distribution with positive skewness. The LN distribution of the final particle sizes is then observed.[27] Thus, the LN distribution of the projected radii we found, combined with the results on the growth kinetics shown in Fig. 4, provides an additional argument that the coarsening is dominated by the SR mechanism.

Conclusions

In this work we investigated changes in the morphology of ligand-capped AuNPs caused by two processes: (i) deposition onto silicon substrate, and (ii) subsequent oxygen plasma treatment of the deposit. We studied deposition of the AuNPs coated with positively and negatively charged as well as uncharged ligands. We found that electrostatic forces between the ligand and substrate are strong enough to displace Au atoms within the core. In the process, the AuNPs undergo plastic deformations and take shapes that can be approximated as spherical caps. The final shape of the particle depends on the charge of the ligand coating. The strongest deformations (flattening) of the NP core were observed for positively charged ligands that are electrostatically attracted to the substrate. The smallest deformations occurred for negatively charged coating that is repelled from the surface.

The plasma treatment affects the morphology of the AuNPs in two ways. First, it makes them coarsen. Second, it changes also the shapes of individual particles. Specifically, we found that their initially flattened shapes become more spherical, resembling droplets of a non-wetting liquid, and their contact angles increase to about 123°. We provided arguments that the growth of the AuNPs during the plasma treatment is dominated by the diffusion-collision mechanism. Our results indicate that during the plasma treatment the particles exhibit a liquid-like behaviour, with the ability to move on the substrate surface and coalesce. To model time evolution of the surface density of the droplets, we employed the mean-field Smoluchowski coagulation rate equation, and assumed that the diffusivity of the droplet scales with its mass as $D(m) \sim m^{-\alpha}$. We found that the experimental data are in accord with the predictions of the Smoluchowski model. Analysis of the droplet density evolution data provided, to our knowledge, for the first time, an estimate of the scaling exponent of $\alpha = 2.6$.

Acknowledgements

This project was operated within the Foundation for Polish Science Team Programme co-financed by the EU European Regional Development Fund Grant no. TEAM/2010-6/4.

Notes and references

1 A. N. Shipway, E. Katz and I. Willner, *ChemPhysChem*, 2000, **1**, 18–52.
2 J.-M. Koo, J.-B. Lee, Y. J. Moon, W.-C. Moon and S.-B. Jung, *J. Phys.: Conf. Ser.*, 2008, **100**, 012034; J. Gun, V. Gutkin, O. Lev, H.-G. Boyen, M. Saitner, P. Wagner, M. D'Olieslaeger, M. H. Abouzar, A. Poghossian and M. J. Schöning, *J. Phys. Chem. C*, 2011, **115**, 4439–4445; K. Raiber, A. Terfort, C. Benndorf, N. Krings and H.-H. Strehblow, *Surf. Sci.*, 2005, **595**, 56–63.
3 J. Gun, D. Rizkov, O. Lev, M. H. Abouzar, A. Poghossian and M. J. Schöning, *Microchim. Acta*, 2009, **164**, 395–404.
4 J. Llorca, A. Casanovas, M. Dominguez, I. Casanova, I. Angurell, M. Seco and O. Rossell, *J. Nanopart. Res.*, 2008, **10**, 537–542.
5 A. Fahmi, A. D'Aléo, R. M. Williams, L. De Cola, N. Gindy and F. Vögtle, *Langmuir*, 2007, **23**, 7831–7835; Y. Maeda, T. Akita,

Open Access Article. Published on 20 February 2014. Downloaded on 4/21/2025 6:47:34 PM.
This article is licensed under a Creative Commons Attribution 3.0 Unported Licence.

M. Daté, A. Takagi, T. Matsumoto, T. Fujitani and M. Kohyama, *J. Appl. Phys.*, 2010, **108**, 094326.
6 K. Ojima, A. Takagi, F. Yamada, T. Matsumoto and T. Kawai, Patent application, 20100233384, 2010.
7 T. F. Jaramillo, S.-H. Baeck, B. Roldan Cuenya and E. W. McFarland, *J. Am. Chem. Soc.*, 2003, **125**, 7148–7149; S. Onoue, J. He and T. Kunitake, *Chem. Lett.*, 2006, **35**, 214–215.
8 K. Winkler, M. Paszewski, T. Kalwarczyk, E. Kalwarczyk, T. Wojciechowski, E. Gorecka, D. Pociecha, R. Holyst and M. Fialkowski, *J. Phys. Chem. C*, 2011, **115**, 19096–19103.
9 P. Thebault, E. Taffin de Givenchy, R. Levy, Y. Vandenberghe, F. Guittard and S. Geribaldi, *Eur. J. Med. Chem.*, 2009, **44**, 717–724.
10 N. R. Jana and X. Peng, *J. Am. Chem. Soc.*, 2003, **125**, 14280–14281.
11 P. W. Voorhees, *J. Stat. Phys.*, 1985, **38**, 231–252; I. M. Lifshitz and V. V. Slyozov, *J. Phys. Chem. Solids*, 1961, **19**, 35–50; C. Wagner, *Z. Electrochem.*, 1961, **65**, 581–591.
12 M. Zinke-Allmang, L. C. Feldman and M. H. Grabow, *Surf. Sci. Rep.*, 1992, **16**, 337–463.
13 A. K. Datye, Q. Xu, K. C. Kharas and J. M. McCarty, *Catal. Today*, 2006, **111**, 59–67.
14 F. Ruffino, V. Torrisi, G. Marletta and M. G. Grimaldi, *Nanoscale Res. Lett.*, 2011, **6**, 112.
15 T. W. Hansen, A. T. Delariva, S. R. Challa and A. K. Datye, *Acc. Chem. Res.*, 2013, **46**, 1720–1730.
16 K. Morgenstern, G. Rosenfeld and G. Comsa, *Phys. Rev. Lett.*, 1996, **76**, 2113–2116; G. Schulze Icking-Konert, M. Giesen and H. Ibach, *Surf. Sci.*, 1998, **398**, 37–48.
17 J. T. Richardson and J. G. Crump, *J. Catal.*, 1979, **57**, 417–425; M. J. J. Jak, C. Konstapel, A. van Kreuningen, J. Verhoeven and J. W. M. Frenken, *Surf. Sci.*, 2000, **457**, 295–310.
18 P. J. F. Harris, *Int. Mater. Rev.*, 1995, **40**, 97–115.
19 M. Smoluchowski, *Phys. Z.*, 1916, **17**, 585–599.
20 W. W. Pai, A. K. Swan, Z. Zhang and J. F. Wendelken, *Phys. Rev. Lett.*, 1997, **79**, 3210–3213.
21 J.-M. Wen, S.-L. Chang, J. W. Burnett, J. W. Evans and P. A. Thiel, *Phys. Rev. Lett.*, 1994, **73**, 2591–2594; C. R. Stoldt, C. J. Jenks, P. A. Thiel, A. M. Cadilhe and J. W. Evans, *J. Chem. Phys.*, 1999, **111**, 5157–5166.
22 K. Kang, S. Redner, P. Meakin and F. Leyvraz, *Phys. Rev. A: At., Mol., Opt. Phys.*, 1986, **33**, 1171–1182; B. C. Hubartt, Y. A. Kryukov and J. G. Amar, *Phys. Rev. E: Stat., Nonlinear, Soft Matter Phys.*, 2011, **84**, 021604.
23 K. Binder and M. H. Kalos, *J. Stat. Phys.*, 1980, **22**, 363–396.
24 K. Morgenstern, G. Rosenfeld, B. Poelsema and G. Comsa, *Phys. Rev. Lett.*, 1995, **74**, 2058–2061.
25 D. S. Sholl and R. T. Skodje, *Phys. Rev. Lett.*, 1995, **75**, 3158–3161; C. DeW. Van Siclen, *Phys. Rev. Lett.*, 1995, **75**, 1574–1577; A. F. Voter, *Phys. Rev. B: Condens. Matter Mater. Phys.*, 1986, **34**, 6819–6829; S. V. Khare, N. C. Bartelt and T. L. Einstein, *Phys. Rev. Lett.*, 1995, **75**, 2148–2151.
26 Y. Chen, R. E. Palmer and J. P. Wilcoxon, *Langmuir*, 2006, **22**, 2851–2855; G. Rizza, H. Cheverry, T. Gacoin, A. Lamasson and S. Henry, *J. Appl. Phys.*, 2007, **101**, 014321; F. Ruffino, R. De Bastiani, M. G. Grimaldi, C. Bongiorno, F. Giannazzo, F. Roccaforte, C. Spinella and V. Raineri, *Nucl. Instrum. Methods Phys. Res., Sect. B*, 2007, **257**, 810–814; F. Ruffino, M. G. Grimaldi, F. Giannazzo, F. Roccaforte, V. Raineri, C. Bongiorno and C. Spinella, *J. Phys. D: Appl. Phys.*, 2009, **42**, 075304; G. Rizza, F. Attouchi, P.-E. Coulon, S. Perruchas, T. Gacoin, I. Monnet and L. Largeau, *Nanotechnology*, 2011, **22**, 175305; E. A. Dawi, A. M. Vredenberg, G. Rizza and M. Toulemonde, *Nanotechnology*, 2011, **22**, 215607.
27 C. G. Granqvist and R. A. Buhrman, *J. Catal.*, 1976, **42**, 477–479.

This journal is © The Royal Society of Chemistry 2014